



A combined laser-induced breakdown and Raman spectroscopy Echelle system for elemental and molecular microanalysis

Marek Hoehse^a, David Mory^d, Stefan Florek^b, Friederike Weritz^a, Igor Gornushkin^{a,*}, Ulrich Panne^{a,c}

^a BAM Federal Institute for Materials Research and Testing, Richard-Willstaetter Str. 11, D-12489 Berlin, Germany

^b ISAS – Institute for Analytical Science, Albert-Einstein-Str. 9, D-12489 Berlin, Germany

^c Humboldt Universitaet zu Berlin, Chemistry Department, Brook-Taylor-Strasse 2, D-12489 Berlin, Germany

^d LTB Lasertechnik Berlin, Rudower Chaussee 29, 12489 Berlin, Germany

ARTICLE INFO

Article history:

Received 7 July 2009

Accepted 19 September 2009

Available online 30 September 2009

Keywords:

LIBS

Raman

Echelle

Laser-induced breakdown spectroscopy

Hyphenated technique

ABSTRACT

Raman and laser-induced breakdown spectroscopy is integrated into a single system for molecular and elemental microanalyses. Both analyses are performed on the same $\sim 0.002 \text{ mm}^2$ sample spot allowing the assessment of sample heterogeneity on a micrometric scale through mapping and scanning. The core of the spectrometer system is a novel high resolution dual arm Echelle spectrograph utilized for both techniques. In contrast to scanning Raman spectroscopy systems, the Echelle–Raman spectrograph provides a high resolution spectrum in a broad spectral range of 200–6000 cm^{-1} without moving the dispersive element. The system displays comparable or better sensitivity and spectral resolution in comparison to a state-of-the-art scanning Raman microscope and allows short analysis times for both Raman and laser induced breakdown spectroscopy. The laser-induced breakdown spectroscopy performance of the system is characterized by ppm detection limits, high spectral resolving power (15,000), and broad spectral range (290–945 nm). The capability of the system is demonstrated with the mapping of heterogeneous mineral samples and layer by layer analysis of pigments revealing the advantages of combining the techniques in a single unified set-up.

© 2009 Elsevier B.V. All rights reserved.

1. Introduction

The chemical and physical heterogeneity of industrial and natural materials presents a serious problem for spectrochemical (micro) analysis. The materials are often complex molecular and elemental multi-component systems which can be disordered in the form of solids, porous solids, and solutions. A comprehensive understanding of their properties and functions can only be obtained by utilizing molecular and elemental information simultaneously. This combination denoted as “hyphenation” in other areas of analytical chemistry integrates complementary, in a mathematical sense orthogonal dimensions of analytical information [1]. While the hyphenation between, for example, chromatographic methods and mass spectrometry is well established, spectrochemical methods are rarely hyphenated in real world applications due to instrumental incompatibilities.

To achieve a powerful yet simple hyphenation, laser-induced breakdown spectroscopy (LIBS) and Raman spectroscopy are promising candidates. Both methods allow fast on-line and in situ analysis without extended sample preparation. LIBS uses short laser pulses to create a microplasma from a material under study. By detecting the

light from the microplasma, elements are identified and their chemical abundances are measured. The technique requires no sample preparation and can be used for analysis of solids, liquids and gases (see e.g. [2] and ref. therein) and yields quantitative information from many minor and trace elements. Molecular information is added through Raman spectroscopy which yields a wealth of vibrational structural information and identifies molecules from vibrational spectra [3]. Raman spectroscopy, however, has a deficit in terms of quantitative analysis which can be compensated through LIBS. Earlier work in hyphenation of the two methods in a sequential instrumental fashion was explored in the areas of geology [4–7], cultural heritage [8–12], remote sensing [13–15], and space exploration [16–20].

The combination is often hampered by instrumental compromises. For example, employing a single pulsed laser for both methods leads to unfavorable signal-to-noise ratios in Raman spectroscopy due to the low duty cycle. In microanalysis, the common focusing and collection optics has to be used for both LIBS and Raman to provide signals from the same spot on the sample under study. In the dispersive part of hyphenated instruments, two spectrometers are frequently used due to different requirements for LIBS and Raman in terms of a spectral range and spectral resolution. Most commonly, two grating spectrometers are employed, one for each technique. Grating spectrometers, however, do not allow the high spectral resolution and

* Corresponding author. Tel.: +49 30 8104 1141; fax: +49 30 8104 1147.

E-mail address: igor.gornushkin@bam.de (I. Gornushkin).

broad spectral range at the same time that are the characteristics vital for LIBS [21–23] and desirable for Raman [3]. In order to cover a broad spectral range with the prescribed resolution, scanning the spectrometer is necessary which ultimately results in prohibitively long measurement times. For LIBS, scanning of the spectrometer is particularly undesirable due to potential sample heterogeneity and impossibility of repetitive probing from the same undisturbed spot. The measurement time for each spectral window includes the time needed for positioning of the grating plus time needed for measurement of the Raman (LIBS) signal. For example, to cover the range of $200\text{--}4000\text{ cm}^{-1}$ with a 0.5-m-grating spectrometer and 1800 groove/mm grating, the grating must be repositioned about 20 times that makes the total acquisition time ~ 100 times longer than that attained with full range (e.g. Echelle) spectrometers. Obviously, the use of Echelle spectrometers in hyphenated LIBS–Raman instruments yields an instant advantage of reducing measurement time and increasing robustness because no moving parts (gratings or prisms) are required. Contrary to LIBS, Echelle spectrometers are rarely used in Raman spectroscopy because of their poor sensitivity and stray light rejection capacity [24,25]. This perception may however prove wrong with the development of a new generation of Echelle spectrometers.

The objective of this work was the development and characterization of a two-laser LIBS–Raman automated microanalysis system equipped with a newly designed dual arm Echelle spectrometer and a single, non-intensified CCD detector. A high spatial resolution of the system was intended to allow elemental and molecular surface mapping on a micrometer scale. In addition, same spot analysis capability allows for layer by layer analysis. High sensitivity of the instrument, especially for Raman spectroscopy with an Echelle system, is ascertained by comparing it to the state-of-the-art commercial Raman microscope.

2. Materials and methods

2.1. Experimental set-up

All experiments were performed with the “Arielle Butterfly” Echelle spectrograph (LTB Lasertechnik Berlin GmbH, Germany), specifically modified to combine LIBS and Raman. The original system was designed for the smart registration of broad range LIBS spectra using two separated spectrometer wings arranged side by side to illuminate one common array detector (focal length of 400 mm, numerical aperture $f/10$, and nominal resolving power, $\lambda/\Delta\lambda$ of 15,000). Each of the wings is a single Echelle spectrograph which can be equipped with individual optical components including its own entrance slit aperture. This compact spectrometer concept is well suited for combined LIBS–Raman analysis because both LIBS and Raman measurements need a sensitive CCD detector with similar specifications but are characterized by different spectroscopic requirements. For advanced LIBS applications, a broad spectral range from the UV to NIR has to be detected with high resolving power of at least $1/10,000$ th of the wavelength to discriminate between thousands of atomic and ionic emission lines. This requires a special design of the Echelle spectrograph with high working order number and a narrow slit width. On the other hand, Raman spectroscopy requires the detection of a weak vibrational spectrum within a relatively narrow spectral range of about 4000 cm^{-1} and medium resolution of about 2 cm^{-1} . This can be advantageously performed using an Echelle spectrograph as well, but with a lower number of orders and a wide slit, i.e. lower $f/\#$ -number. In summary, for LIBS the high resolving power of the Echelle grating is exploited, whereas in Raman spectroscopy the high optical throughput of the Echelle spectrograph is utilized.

Fig. 1 displays the schematic of the LIBS–Raman set-up. For LIBS, a frequency doubled Nd:YAG laser (max 200 mJ pulse energy at 532 nm, 7 ns pulse duration, Surelite II, Continuum, Germany)

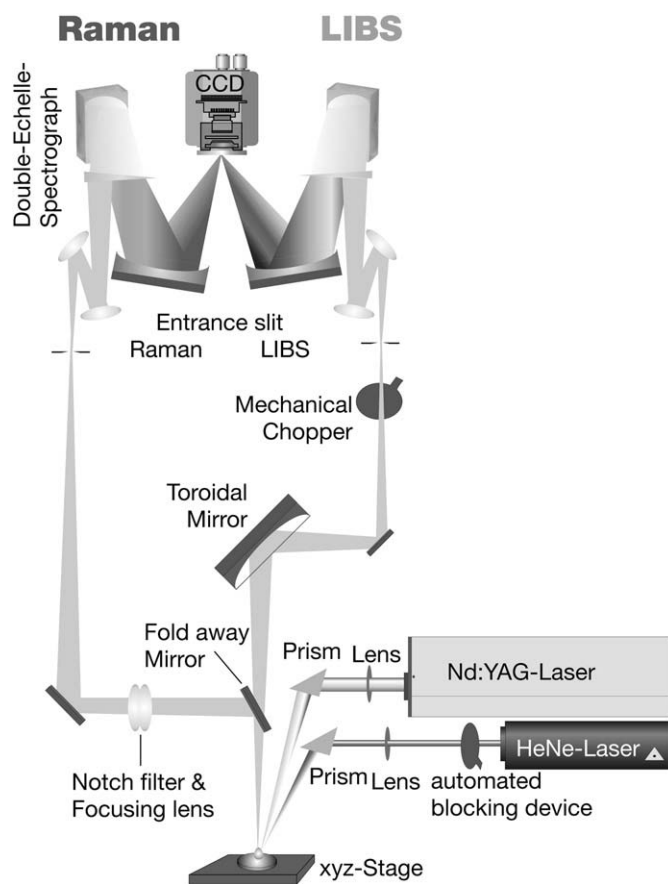


Fig. 1. Schematic diagram of the experimental LIBS–Raman set-up.

operating at 10 Hz is focused (laser aplanat, $f=75\text{ mm}$, CVI Melles Griot, USA) on the sample surface at an angle of 8° with respect to the surface normal. The resulting diameter of the laser beam on the surface is about $50\text{ }\mu\text{m}$ yielding an irradiance of $1.8 \times 10^{11}\text{ W/cm}^2$. The plasma emission is collected in top view geometry by an inclined toroidal ($f=110\text{ mm}$) and folding mirrors (all with a UV-enhanced Al/SiO₂ layer) and guided through the $50 \times 50\text{ }\mu\text{m}^2$ entrance slit system into the LIBS branch of the spectrometer. For this slit width, the practical resolving power is about 15,000 (see below). The Echelle spectrum pattern is fragmented into 61 orders which cover the total wavelength range from 290 nm to 945 nm. Compared to LIBS Echelle systems reported earlier [21–23], the spectral range was shifted here into the NIR region to allow the observation of NIR lines of non-metals. The spectrograph is equipped with the CCD camera with 1024×256 pixels and $26\text{ }\mu\text{m}$ pitch (Newton DU 920N-BRDD, Andor Technology, Northern Ireland). To prevent the CCD detecting early continuum radiation from the LIBS plasma, a mechanical chopper is used in front of the entrance slit which cuts off an initial portion of the plasma radiation [22].

For Raman, the He–Ne laser line 632.8 nm (25 LHP-928-230, 35 mW, Melles Griot, USA) is focused on the sample (spot size diameter $\sim 50\text{ }\mu\text{m}$) providing the irradiance of $1.5 \times 10^9\text{ W/cm}^2$. The scattered light is guided by achromatic doublets ($f=83\text{ mm}$, 3-fold magnification) through the entrance slit ($120 \times 200\text{ }\mu\text{m}$) of the Raman branch of the spectrometer. Due to the $200\text{ }\mu\text{m}$ wide entrance slit, the practical resolving power is about 10,000, i.e. 1.35 cm^{-1} at 700 nm ($14,300\text{ cm}^{-1}$). The simultaneous wavelength range spans more than 4500 cm^{-1} segmented into only 28 Echelle orders. The Raman signal is detected with the same CCD. Rayleigh scattering is rejected by long pass filters (LP02-633RE-25, Semrock, USA) transparent above 79 cm^{-1} with respect to the laser line. Except for the two entrance orifices, the system is completely encased to maximally reject ambient light.

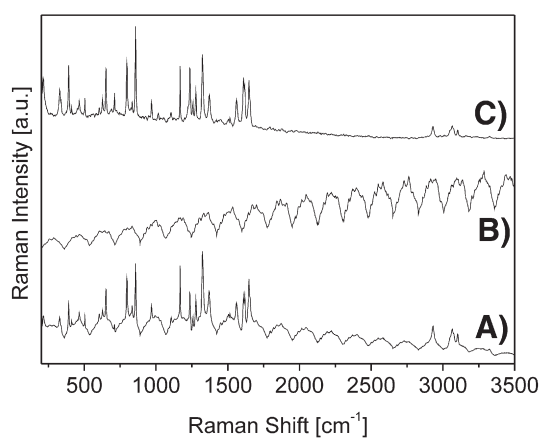


Fig. 2. Blaze correction of Echelle Raman spectra. A) Raw spectrum of paracetamol (exposure time 1 s, binning 8). B) Tungsten lamp spectrum used for blaze correction. C) Blaze function corrected spectrum of paracetamol.

Spatial resolution is important for mapping and, therefore, for the assessment of sample heterogeneity. A spatial resolution of around 50 μm for LIBS was determined by measuring laser crater diameters from scanning electron microscopy images (ESEM XL 30, FEI, USA). To determine the spatial resolution for the Raman system, a CCD was placed in the focal plane of the focusing lens to image the He–Ne laser beam weakened by neutral density filters. The determined spot size was also about 50 μm .

The system is fully automated to allow fast LIBS–Raman sample surface mapping. All the components including the *xyz*-stage (rds motion, Germany, accuracy $\leq 1 \mu\text{m}$, travel range 100 mm), folding mirror, and beam stop for the He–Ne laser are driven by a computer or small electronic circuits. A user defined area is rastered automatically in any preferred way. In mapping experiment, specified points on a sample surface are memorized and measured one after another by the Raman branch of the spectrometer. Then, the spectrometer is automatically switched to the LIBS arm whereby the He–Ne laser is blocked and the beam folding mirror (see Fig. 1) is displaced from its initial position to open the optical path for LIBS. The Nd:YAG laser is triggered by the mechanical chopper instantly activated while the translation stage automatically returns to the positions used previously in Raman, thus enabling the collection of LIBS spectra from exactly the same spots as in Raman. It is also possible to switch between Raman and LIBS after every measurement.

A state-of-the-art Raman microscope (LabRAM HR800, Jobin Yvon, Bensheim, Germany; BX41 microscope, Olympus, Hamburg, Germany) was used to verify the high quality of Raman spectra obtained with our instrument. All Raman spectra were obtained here by the excitation with a He–Ne laser (max. 6 mW) that was focused on the

sample surface (spot size diameter $\sim 10 \mu\text{m}$) by a 10 \times microscope objective (N.A. 0.25).

2.2. Spectra processing

Raman and LIBS spectra obtained are corrected for the Echelle blaze function. The blaze function characterizes an Echelle grating response that is maximal at the grating blaze angle and decreases with the deviation from this angle. In the presence of fluorescence background, a raw Echelle spectrum features a structured background as revealed in Fig. 2A for a paracetamol reference sample. A correction can be realized either computationally or experimentally using continuous light correction. The computational approach is less adequate because calculations are performed only for optics situated inside the spectrometer, while the experimental correction takes into account all optical elements. Fig. 2B shows the corresponding tungsten lamp spectrum utilized for the correction, while Fig. 2C gives the corrected spectrum of paracetamol, where spectral artifacts are efficiently removed upon the correction.

For the comparison of the Echelle Raman performance, spectra were normalized to noise determined from 50 repetitive measurements. As the observed noise of the spectra obtained with the Echelle system varies a little with the spectral range (higher for lower wave numbers, lower for higher wave numbers), averaging the noise over the complete spectral range would deliver incorrect results. Thus the considered spectral band was normalized to noise measured close to the observed Raman signal.

In case of the LIBS–Raman mapping, the maps were compiled using MATLAB (The Mathworks, Version 7.3.).

2.3. Samples

Mineral samples of different origin were used and are characterized in the supplementary information (see Appendix SI 1). All samples were cut in slices and polished. For the determination of detection limits for LIBS, steel standard materials (SS401/1–SS405/1 SS406–SS409, Bureau of Analyzed Samples, Ltd., UK) were employed. For comparison of the Raman performance and the correction of the Echelle blaze function, wavelength calibration substances such as sulfur from Sigma Aldrich (USA), a silicon wafer, and paracetamol from Ratiopharm (Germany) were used. The analysis of pigment layers was done with layers of pure acrylic paints (Heavy Body Acrylic Color Lines, GOLDEN, USA), coated on chalk covered wood.

3. Results and discussion

As mentioned above, Echelle spectrographs are widely used in LIBS but only rarely in Raman due to their relatively low throughput and poor stray light rejection. However, the new generation of Echelle spectrographs equipped with sensitive CCDs and employed in

Table 1
Comparison of Raman benchmark data and performances.

	Echelle–Raman Binning 8	Echelle–Raman Binning 4	Raman microscope 300 gr/mm	Raman microscope 1800 gr/mm
Detector	Thermoelectrically cooled CCD			
Dark current [$e^-/\text{pix}/\text{h}$]	~ 100 at -90°C			
Magnification	3 \times			
Aperture angle	32 $^\circ$			
Grating	Echelle			
Binning on CCD	8	4	300 gr/mm	1800 gr/mm
Spotsize	50 μm			
Irradiance [W/cm^{-2}]	1500			
Pixel resolution [$\text{cm}^{-1}/\text{pixel}$]	2.09	1.05	1.95	0.31
FWHM [cm^{-1}]	2.8	1.4	6.6	0.9
Number of spectral windows	1	1	2	18
Measurement time (full spectrum, exp. time 1 \times 1 s)	1 s	1 s	15 s	105 s

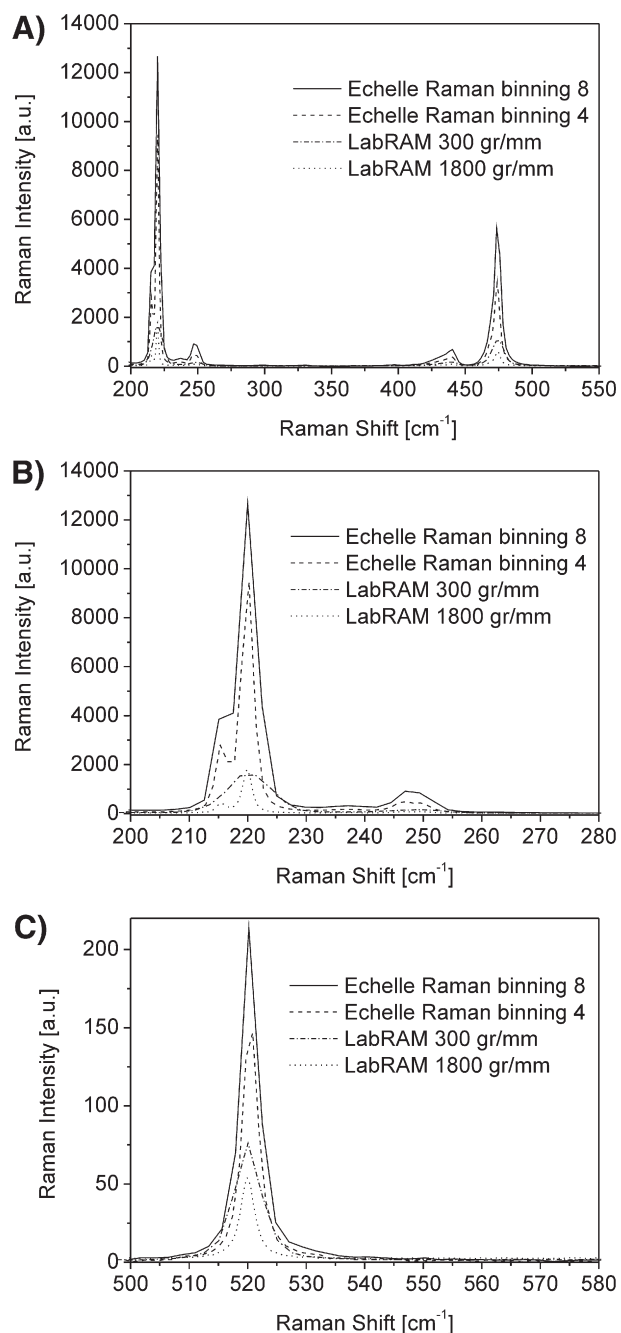


Fig. 3. Comparison of Echelle and grating Raman spectrograph. A) Spectra of sulfur for Echelle Raman (binning 8 and 4 pixels) and for LabRAM HR800 (gratings: 300 gr/mm and 1800 gr/mm), all normalized to noise, exposure times: 50×1 s. B) close up of the 220 cm^{-1} sulfur peak showing differences in true resolution. C) Spectra of Silicon for Echelle Raman (binning 8 and 4 pixels) and for LabRAM HR800 (gratings: 300 gr/mm and 1800 gr/mm), all normalized to noise, exposure times: 50×1 s.

combination with notch filters are capable to deliver a performance comparable with that of best commercial Raman grating instruments. We will not discuss in detail advantages of the Echelle-LIBS system as similar systems have already been reported [22,23,26–29], but put emphasis on the Echelle-Raman system.

3.1. Echelle-Raman performance

The high resolution provided by the Echelle spectrograph employed here is excessive for Raman measurements; therefore it can be traded for a higher sensitivity by means of binning horizontal

pixels on the CCD detector or enlarging the size of the entrance slit. The possibility of changing the horizontal CCD pixel binning enables a change of the resolution without the need for adjustment in the optical system and, thus, without further calibration. To assure high quality Raman spectra, the Raman branch of our spectrograph was compared to a state-of-the-art grating-spectrograph Raman microscope. The purpose of the comparison was to assert the competitiveness of Echelle spectrographs with respect to conventional grating spectrometers.

The two spectrographs are equipped with different optics that makes comparison difficult. In our spectrograph, light is focused and collected with a system of lenses, while in the LabRAM with a microscope objective. The intensity of the collected Raman signal depends on both the focusing optics and sample opacity that determine the penetration depth [3]. The microscope objective has a short focal length and large numerical aperture and, therefore, a shallow penetration depth. The focusing optics in the Echelle spectrograph has in contrary the longer focal length and smaller collection angle resulting in the larger penetration depth. To make the comparison adequate for all samples under study, the low magnification $10\times$ objective ($\sim 10 \mu\text{m}$ spot size diameter) was used in the LabRAM as it provided focusing/collection parameters similar to those in the Echelle system. Additionally, the same laser irradiance was employed to provide similar excitation conditions for Raman measurements.

Table 1 compares instrumental parameters of the two Raman setups. The CCD in the Raman microscope is cooled with liquid nitrogen that provides 50 times lower dark current compared to that of the thermoelectrically cooled Echelle-Raman CCD detector. This, however, does not result in better signal-to-noise ratio of the Raman microscope system (see below). The Echelle-Raman system allows the direct measurement of Raman spectra in a range of $200\text{--}6000 \text{ cm}^{-1}$, whereas from 2 to 18 scans are needed for the Raman microscope to cover the smaller but sufficient Raman range of $200\text{--}4000 \text{ cm}^{-1}$. Depending on the used grating, it might take ~ 100 times longer to measure a similar resolution Raman spectrum with the LabRAM than with the Echelle-Raman system.

Fig. 3 depicts Raman spectra averaged over 50 measurements of sulfur and silicon, suitable standard materials to compare the Raman performance of the two spectrographs. All spectra are measured with 1 s of the exposure time per spectral window and are normalized to noise as explained above. For sulfur, the Echelle-Raman system yields a three to nine-fold better signal-to-noise ratio than the Raman microscope depending upon the compared resolutions.

As seen from Fig. 3B, the LabRAM with the 300 gr/mm grating does not resolve two sulfur signals at 214 and 219 cm^{-1} even though the theoretical pixel resolution is similar to that of the Echelle-Raman with 8-pixel binning. It becomes possible only with the 1800 gr/mm grating in a scanning mode. The Echelle-Raman system, in contrary, discerns the signals even with the 8-pixel binning (the 219 cm^{-1} band is seen as a shoulder in Fig. 3B) and resolves them distinctly with the 4-pixel binning. Fig. 3C displays Raman spectra of silicon, a material with high opacity compared to sulfur. The results are comparable to the sulfur measurements: the Echelle-Raman system yields again a two to four-fold better signal-to-noise ratio than the microscope system.

3.2. LIBS performance

The performance of a similar Echelle-LIBS system is described elsewhere [22,29]. In brief, the spectral resolving power of the spectrograph was 15,000 over the whole spectral range ($300\text{--}935 \text{ nm}$) verified by using a mercury lamp as a line source. The limits of detection (LOD) were determined exemplarily for Cu and Cr as 0.005 % and 0.012 % correspondingly, using steel reference materials and Cu(I) 327.40 nm and Cr(I) 425.44 nm lines. A typical

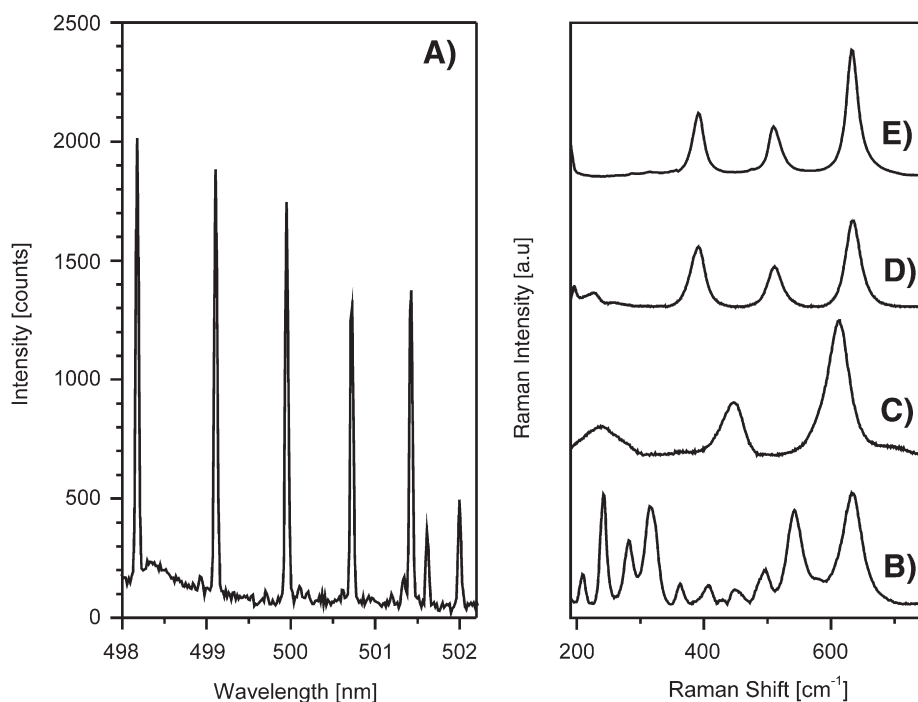


Fig. 4. Identification of Polymorphic forms of TiO_2 . A) Titanium in LIBS spectrum of copper ore. b–d) Raman spectra of brookite (B), rutile (C), and anatase (D) [33]. E) Raman spectrum of anatase obtained from same spot as in A (exposure time 10 s).

measurement precision was $\sim 5\%$ RSD over the entire concentration range. The measurements were performed with 10 laser pulses delivered to the same spot without translating the sample (1 s exposure time, 10 Hz, $1.8 \times 10^{11} \text{ W/cm}^2$). The LODs could further be improved by higher irradiances, longer integration times, and translation of the sample, although the reported LODs are typical for microanalysis [22,30].

3.3. LIBS/Raman spectra

As mentioned above, LIBS and Raman provide complementary information allowing for a solution of analytical problems which cannot be solved by either of the techniques alone. In contrary to LIBS, Raman scattering cannot be detected in every sample spot on every material due to the weak cross section of a Raman signal and due to interfering fluorescence.

The supplementary information SI 1 summarizes the results of Raman–LIBS analysis of six heterogeneous mineral samples. Due to differences in the Raman scattering cross sections and orientation of microcrystalline areas, Raman spectra of heterogeneous materials do not necessarily originate from the whole illuminated spot as contrasted to LIBS. Thus, the number of elements revealed by LIBS can be larger than that predicted by Raman spectroscopy after identification of the molecular compound from the Raman spectrum. Hence, LIBS offers additional, potentially quantitative information useful for sample identification or differentiation between similar samples.

The benefit from the combination of LIBS and Raman can be bidirectional. For example, as it can be seen in SI 1, different investigated samples contain quartz which could be identified by Raman. But because Raman spectra of quartz are similar for all the minerals, they could not be sufficient basis for differentiating the minerals. Here LIBS comes to help: LIBS spectra taken from the same sample spots as the Raman spectra show significant differences in the elemental composition due to impurities, making the differentiation easy.

On the other hand, LIBS by itself cannot provide information on the structure of materials with identical composition. For example, in analysis of polymorphous materials (e.g. TiO_2 polymorphs) the benefits offered by Raman become obvious. Such analysis is important for pharmaceutical industry [31] or catalysis [32]. This point is illustrated by Fig. 4A which reveals a fragment of the LIBS spectrum obtained from a copper ore. Among spectral lines from other elements,

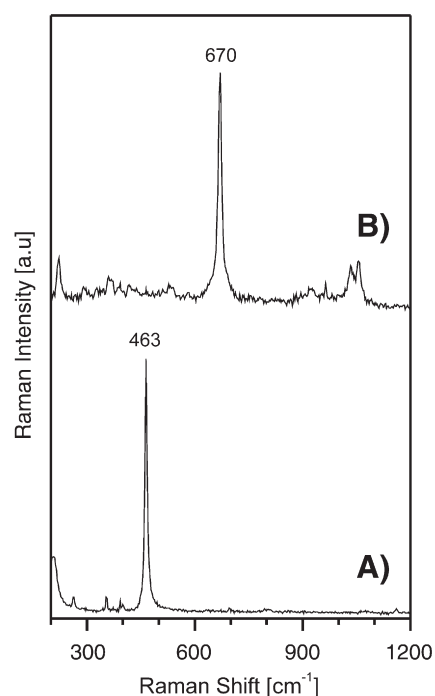


Fig. 5. Spectra of two minerals (exposure time 10 s, binning 8) obtained in the same ore. A) Spectrum of Quartz. B) Spectrum of Tremolite.

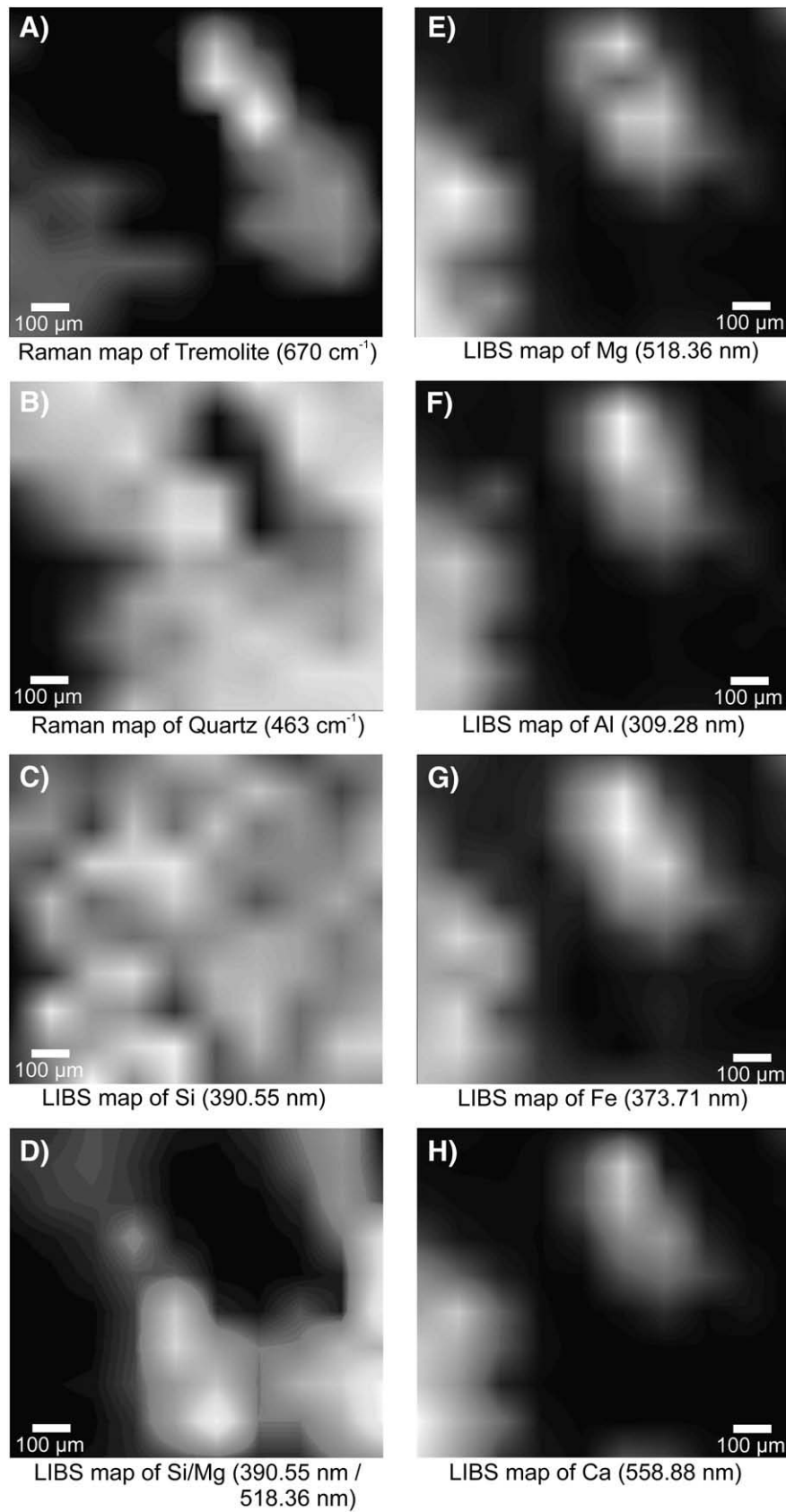


Fig. 6. Raman (A–B) and LIBS (C–H) maps of a mineral, obtained from similar sample area of an ore.

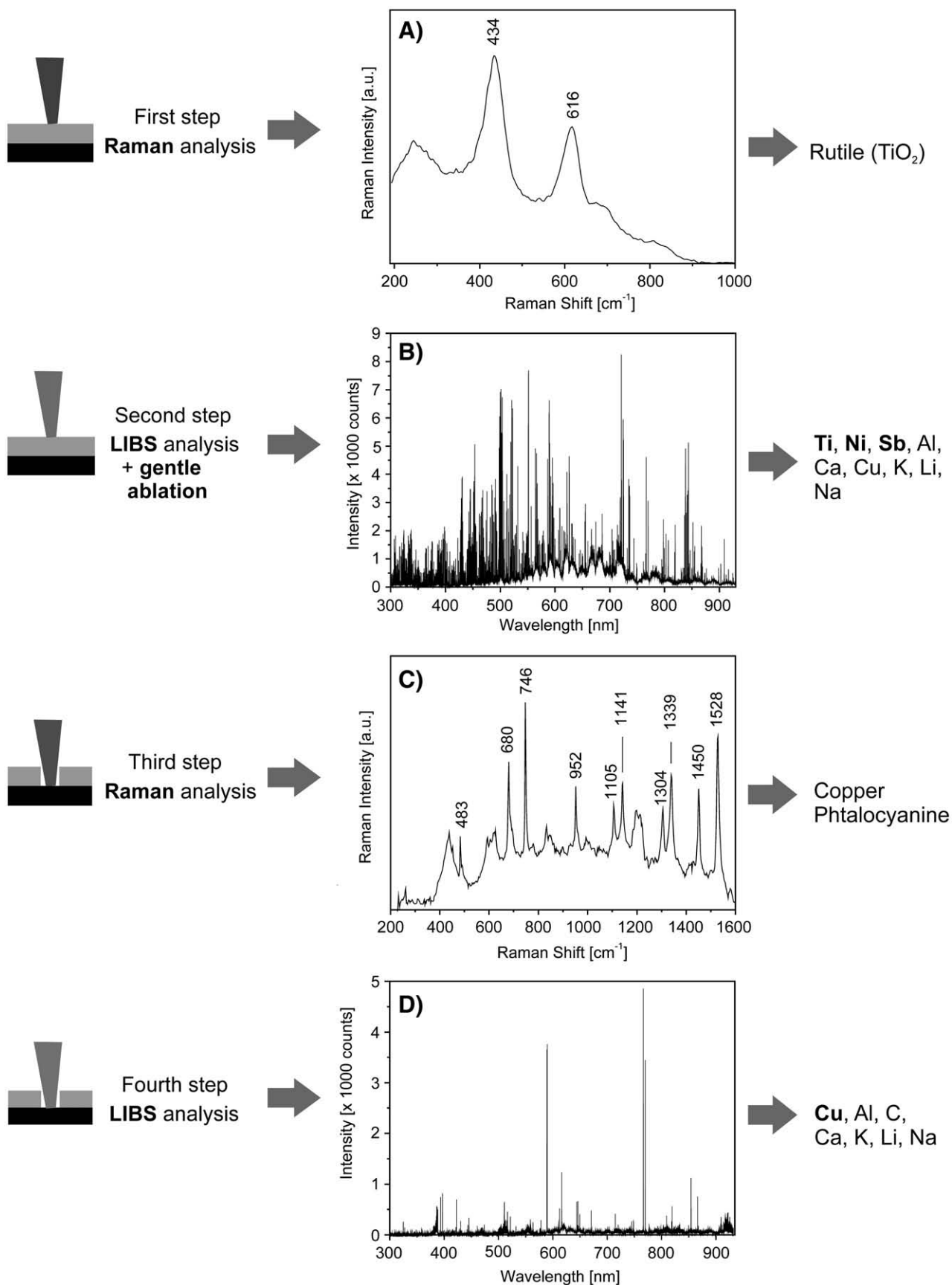


Fig. 7. Layer by Layer LIBS–Raman analysis. A) Raman analysis of the top layer (1 s, 1500 W/cm²). B) LIBS analysis of the top layer (1 s, pulse energy 50 mJ). C) Raman analysis of bottom layer (50 s, 150 W/cm²) D) LIBS analysis of bottom layer (1 s, pulse energy 50 mJ).

high intensities of titanium spectral lines indicate the likely presence of TiO₂. However, LIBS is not able to discern the existing polymorphic forms of TiO₂ (anatase, rutile, brookite) because they yield identical spectra. Here Raman comes to help: Fig. 4B shows that Raman spectroscopy is well capable of distinguishing the polymorphs [33]. The Raman spectrum taken from the same spot as the LIBS spectrum shows that the origin of titanium in the studied copper ore is anatase (Fig. 4E). Thus, Raman spectroscopy helps to interpret LIBS results and to complete the analytical picture.

3.4. LIBS–Raman mapping

An iron ore sample was used for preliminary mapping experiments. An area of 1 mm² was scanned; the distance between each measurement point was 100 μm. Fig. 5 shows the Raman spectra of two different inclusions, quartz and tremolite, obtained from the mapped area. The exposure time for each measurement was 10 s. The strongest background-corrected Raman signals at 463 cm⁻¹ and 670 cm⁻¹ for quartz and tremolite respectively (symmetric Si–O–Si stretching vibrations) were used for Raman mapping.

Following the Raman measurements, the same sample points were measured by LIBS (exposure time 500 μs). One line per element was used: Si(I) 390.55 nm, Mg(I) 518.36 nm, Al(I) at 309.28 nm, Fe(I) 373.71 nm, and Ca(I) at 558.88 nm. Fig. 6 displays the results of the Raman and LIBS mapping. The grey scale reflects the intensities of measured signals (and, thereby, concentrations): the transition from white to black corresponds to the transition from high to low signal intensities.

The Raman maps in Fig. 6A and B depict the distributions of quartz and tremolite on the tested 1 mm² area of the iron ore sample. These maps are complemented by the LIBS maps (Fig. 6C–H) which display the distributions of elemental constituents. A comparison of Fig. 6A–B and C–H reveals that the elements Mg, Al, Fe, and Ca are associated with tremolite, whereas the elemental map of the quartz-containing areas consists of mostly silicon. This indicates the relative purity of quartz and its freedom from the presence of concomitant elements. As silicon is contained in both minerals, its line is detected over the entire mapped area (Fig. 6C). Based on the information obtained, we conclude that the distribution of quartz in the iron ore can in principle be detected by LIBS alone: quartz is contained in areas which show high emission signal from silicon and not from Fe, Mg, Ca, or Al. The comparison of the Raman map for quartz (Fig. 6A) with the LIBS map for Si/Mg ratio (Fig. 6D) demonstrates this point experimentally. Thus, understanding of sample composition is feasible through combined LIBS–Raman.

3.5. Layer by layer analysis

The combination of LIBS and Raman opens up more possibilities than just providing elemental and molecular information from a sample surface. It can be also used for depth profiling, for example, for profiling paint layers or coatings. The benefit of the LIBS–Raman combination includes the possibility of penetrating through top layers to expose and detect Raman and LIBS signals from layers underneath. The Nd:YAG laser can serve here two purposes: operating with high irradiances, the laser generates the plasma for LIBS measurement, and operating at low irradiances the laser can be used for a gentle sample ablation. The optimal ablation irradiance depends on the ablation threshold of the top layer and photostability of the second layer. If the bottom layer consists, for example, of robust inorganic pigments like rutile in Titanium White, the Raman scattering of rutile is detectable even after drilling the sample at high irradiance that creates a plasma and allows simultaneous LIBS measurements. However, the more sensitive layers such as organic pigments demand low irradiances for ablation that are far below the plasma formation threshold. Fig. 7 highlights an example of this approach for analysis of layered acrylic

paints commonly used in cultural heritage. Compared to conventional paint layer analysis (where a chip of paint is removed for analysis with a scalpel), this method is less destructive as the crater diameter is only about 100 μm. In our experiment, the pigment in the top layer consisted of Titanate Yellow, a mixture of inorganic oxides of Ti, Ni, and Sb that are hard to vaporize and therefore a higher irradiance was needed. The bottom layer consisted of PB15:4, a more sensitive organic pigment that belongs to the group of copper phthalocyanines.

First, the top layer (Titanate Yellow) was investigated with Raman spectroscopy, revealing signals from rutile (Fig. 7A). The result, however, was not decisive as other pigments contained rutile as well. Applying LIBS, the Raman results were clarified (Fig. 7B): the presence of Ni and Sb in LIBS spectrum indicated the layer to be Titanate Yellow. Further, the Nd:YAG laser was employed afterwards for optical ablation of the top layer until reaching the bottom layer. To reach the bottom layer (the thickness of the top layer was ~50 μm) it took about 300 s of drilling at an irradiance of 2×10^8 W/cm². This was followed by Raman/LIBS investigations of the bottom layer. The Raman spectrum displayed the features of the Copper Phthalocyanine PB15:4 (Fig. 7C), whereas LIBS measurement proves the presence of Cu (Fig. 7D).

The example illustrates that the LIBS/Raman combination is beneficial for layer by layer analyses, however, care has to be taken to optimize ablation conditions accordingly.

4. Conclusions

A novel LIBS–Raman instrument based on a double-arm Echelle spectrograph has been constructed and characterized. The instrument assures optimal detection conditions for both the spectroscopic techniques. Further, we have demonstrated that Echelle spectrographs are suitable for Raman measurements and are competitive in sensitivity and resolution compared to the state-of-the-art commercial grating Raman spectrographs. The distinct advantage of the Echelle systems is their ability to image the complete Raman spectral range (200–4000 cm⁻¹) without scanning a dispersive element.

We have also shown that LIBS–Raman mapping of heterogeneous materials is beneficial for a comprehensive material characterization. Due to the complementary nature of the two methods, information obtained by the two techniques adds to a comprehensive analytical picture. The Raman technique reveals the occurrence of molecular structures (i.e. mineral inclusions) whereby the LIBS technique maps elemental distributions and helps to find elements associated with certain minerals. The layer by layer analysis enables the Raman and LIBS detection of each layer with minimal sample destruction.

Additionally, a combined data treatment (data fusion) could improve the discriminating power of the LIBS/Raman combination as compared to separate treatment of the data obtained by each of the techniques.

Acknowledgments

We gratefully acknowledge funding of this research by the BMWi MNPOgrant 21/06. The authors wish to sincerely thank the LIBS team of Lasertechnik Berlin (LTB) for technical support, Klaus-Jürgen Wenzel (BAM) for valuable assistance in this project, and Dr. Heike Stege (Doerner Institut, Munich, Germany) for providing the paint samples.

Appendix A. Supplementary data

Supplementary data associated with this article can be found in the online version, at doi: [10.1016/j.sab.2009.09.004](https://doi.org/10.1016/j.sab.2009.09.004).

References

- [1] T. Hirschfeld, R. Crawford, C. Wong, R. Sanborn, Hyphenated IR Techniques, Abstr. Pap. Am. Chem. S., vol. 180, 1980, 113-ANYL.
- [2] C. Pasquini, J. Cortez, L.M.C. Silva, F.B. Gonzaga, Laser induced breakdown spectroscopy, *J. Braz. Chem. Soc.* 18 (2007) 463–512.
- [3] R.L. McCreery, *Raman Spectroscopy for Chemical Analysis*, John Wiley & Sons, New York, 2000.
- [4] D. Derome, M. Cathelineau, C. Fabre, M.-C. Boiron, D. Banks, T. Lhomme, M. Cuney, Paleo-fluid composition determined from individual fluid inclusions by Raman and LIBS: application to mid-proterozoic evaporitic Na–Ca brines (Alligator Rivers Uranium Field, northern territories Australia), *Chem. Geol.* 237 (2007) 240–254.
- [5] D. Derome, M. Cuney, M. Cathelineau, C. Fabre, J. Dubessy, P. Bruneton, A. Hubert, A detailed fluid inclusion study in silicified breccias from the Kombolgie sandstones (Northern Territory, Australia): inferences for the genesis of middle-Proterozoic unconformity-type uranium deposits, *J. Geochem. Explor.* 80 (2003) 259–275.
- [6] C. Fabre, M.C. Boiron, J. Dubessy, M. Cathelineau, D.A. Banks, Palaeofluid chemistry of a single fluid event: a bulk and in-situ multi-technique analysis (LIBS, Raman Spectroscopy) of an Alpine fluid (Mont-Blanc), *Chem. Geol.* 182 (2002) 249–264.
- [7] B.J. Marquardt, D.N. Stratis, D.A. Cremers, S. Michael Angel, Novel probe for laser-induced breakdown spectroscopy and Raman measurements using an imaging optical fiber, *Appl. Spectrosc.* 52 (1998) 1148–1153.
- [8] M. Bicchieri, M. Nardone, P.A. Russo, A. Sodo, M. Corsi, G. Cristoforetti, V. Palleschi, A. Salvetti, E. Tognoni, Characterization of azurite and lazurite based pigments by laser induced breakdown spectroscopy and micro-Raman spectroscopy, *Spectrochim. Acta Part B* 56 (2001) 915–922.
- [9] R. Bruder, V. Detalle, C. Coupry, An example of the complementarity of laser-induced breakdown spectroscopy and Raman microscopy for wall painting pigments analysis, *J. Raman Spectrosc.* 38 (2007) 909–915.
- [10] L. Burgio, K. Melessanaki, M. Doulgeridis, R.J.H. Clark, D. Anglos, Pigment identification in paintings employing laser induced breakdown spectroscopy and Raman microscopy, *Spectrochim. Acta Part B* 56 (2001) 905–913.
- [11] M. Castillejo, M. Martin, M. Oujja, D. Silva, R. Torres, C. Domingo, J.V. Garcia-Ramos, S. Sanchez-Cortes, Spectroscopic analysis of pigments and binding media of polychromes by the combination of optical laser-based and vibrational techniques, *Appl. Spectrosc.* 55 (2001) 992–998.
- [12] I. Osticioli, N. Mendes, S. Porcinai, A. Cagnini, E. Castellucci, Spectroscopic analysis of works of art using a single LIBS and pulsed Raman setup, *Anal. Bioanal. Chem.* 394 (2009) 1033–1041.
- [13] S.K. Sharma, A.K. Misra, P.G. Lucey, R.C. Wiens, S.M. Clegg, Combined remote LIBS and Raman spectroscopy at 8.6 m of sulfur-containing minerals, and minerals coated with hematite or covered with basaltic dust, *Spectrochim. Acta Part A* 68 (2007) 1036–1045.
- [14] R.C. Wiens, S.K. Sharma, J. Thompson, A. Misra, P.G. Lucey, Joint analyses by laser-induced breakdown spectroscopy (LIBS) and Raman spectroscopy at stand-off distances, *Spectrochim. Acta Part A* 61 (2005) 2324–2334.
- [15] S.K. Sharma, A.K. Misra, P.G. Lucey, R.C.F. Lentz, A combined remote Raman and LIBS instrument for characterizing minerals with 532 nm laser excitation, *Spectrochim. Acta Part A* 73 (2009) 468–476.
- [16] H.W. Hubble, M. Ghosh, S.K. Sharma, K.A. Horton, P.G. Lucey, S.M. Angel, R.C. Wiens, A combined remote LIBS and Raman spectroscopic study of minerals, *Lunar Planet. Sci.* XXXIII (2002).
- [17] J. Thompson, R. Wiens, S. Sharma, P. Lucey, A. Misra, Combined remote LIBS and Raman spectroscopy measurements, *Lunar Planet. Sci.* XXXVI (2005).
- [18] S.M. Clegg, R.C. Wiens, S.K. Sharma, P. Lucey, A. Misra, J. Barefield, LIBS–Raman spectroscopy of minerals using remote surface modification technique, *Lunar Planet. Sci.* XXXVII (2006).
- [19] G.B. Courreges-Lacoste, B. Ahlers, F.R. Perez, Combined Raman spectrometer/laser-induced spectrometer for the next ESA mission to breakdown Mars, *Spectrochim. Acta Part A* 68 (2007) 1023–1028.
- [20] C.B. Dreyer, G.S. Mungas, P. Thanh, J.G. Radziszewski, Study of sub-mj-excited laser-induced plasma combined with Raman spectroscopy under Mars atmosphere-simulated conditions, *Spectrochim. Acta Part B* 62 (2007) 1448–1459.
- [21] R.E. Neuhauser, B. Ferstl, C. Haisch, U. Panne, R. Niessner, Design of a low-cost detection system for laser-induced plasma spectroscopy, *Rev. Sci. Instrum.* 70 (1999) 3519–3522.
- [22] M. Mueller, I.B. Gornushkin, S. Florek, D. Mory, U. Panne, Approach to detection in laser-induced breakdown spectroscopy, *Anal. Chem.* 79 (2007) 4419–4426.
- [23] C. Haisch, U. Panne, R. Niessner, Combination of an intensified charge coupled device with an echelle spectrograph for analysis of colloidal material by laser-induced plasma spectroscopy, *Spectrochim. Acta Part B* 53 (1998) 1657–1667.
- [24] M.J. Pelletier, Raman spectroscopy using an echelle spectrograph with CCD detection, *Appl. Spectrosc.* 44 (1990) 1699–1705.
- [25] J.V. Sweedler, Charge transfer device detectors and their applications to chemical analysis, *CRC Crit. Rev. Anal. Chem.* 24 (1993) 59–98.
- [26] C. Haisch, H. Becker-Ross, An electron bombardment CCD-camera as detection system for an echelle spectrometer, *Spectrochim. Acta Part B* 58 (2003) 1351–1357.
- [27] I. Radivojevic, C. Haisch, R. Niessner, S. Florek, H. Becker-Ross, U. Panne, Microanalysis by laser-induced plasma spectroscopy in the vacuum ultraviolet, *Anal. Chem.* 76 (2004) 1648–1656.
- [28] M. Sabsabi, V. Detalle, A. Harith Mohamed, W. Tawfik, H. Imam, Comparative study of two new commercial echelle spectrometers equipped with intensified CCD for analysis of laser-induced breakdown spectroscopy, *Appl. Opt.* 42 (2003) 6094–6098.
- [29] S. Florek, C. Haisch, M. Okruss, H. Becker-Ross, A New, Versatile Echelle Spectrometer Relevant to Laser Induced Plasma Applications, 1st International Conference on Laser-Induced Plasma Spectroscopy and Applications (LIBS 2000), Pergamon-Elsevier Science Ltd, Tirrenia, Italy, 2000, pp. 1027–1034.
- [30] I. Radivojevic, R. Niessner, C. Haisch, S. Florek, H. Becker-Ross, U. Panne, Detection of bromine in thermoplasts from consumer electronics by laser-induced plasma spectroscopy, *Spectrochim. Acta Part B* 59 (2004) 335–343.
- [31] P.H. Karpinski, Polymorphism of active pharmaceutical ingredients, *Chem. Eng. Technol.* 29 (2006) 233–237.
- [32] K. Kontapakdee, J. Panpranot, P. Praserttham, Effect of Ag addition on the properties of Pd-Ag/TiO₂ catalysts containing different TiO₂ crystalline phases, *Catal. Commun.* 8 (2007) 2166–2170.
- [33] R.T. Downs, The RRUFF Project: An Integrated Study of the Chemistry, Crystallography, Raman and Infrared Spectroscopy of Minerals, Program and Abstracts of the 19th General Meeting of the International Mineralogical Association, Kobe, Japan, 2006.